Fluctuating Noise Drives Brownian Transport

Yoshihiko Hasegawa and Masanori Arita

Department of Biophysics and Biochemistry, Graduate School of Science,

The University of Tokyo, Tokyo 113-0033, Japan

(Dated: Sep 13, 2012)

Abstract

The transport properties of Brownian ratchet was studied in the presence of stochastic intensity noise (SIN) in both overdamped and underdamped regimes. In the overdamped case, analytical solution using the matrix continued fraction method revealed the existence of a maximum current when the noise intensity fluctuates on intermediate time scale regions. Similar effects were observed for the underdamped case by Monte Carlo simulations. The optimal time-correlation for the Brownian transport coincided with the experimentally observed time-correlation of the extrinsic noise in *Esherichia coli* gene expression and implied the importance of environmental noise for molecular mechanisms.

1. INTRODUCTION

Noise-induced phenomena are attracting much attention not only in engineering but also in molecular biology. Counter-intuitively, noise can enhance system performance by increasing transmission and synchronization of information through stochastic resonance [1–6] and noise-induced synchronization [7–10].

For example, molecular systems function efficiently in nano-scale environments under multi-scale noise through thermal and other environmental fluctuations [11–14]. This efficiency should not be interpreted by assuming steady-state or Gaussian distribution. A recent single-cell observation of *Escherichia coli* revealed that the protein copy number does not obey the gamma distribution [15], and its stationary distribution can be approximated by superstatistics (i.e., the superposition of multiple statistical models; see Equation 1 and Discussion). Chabot *et al.* revealed that the cellular variability in gene expressions comes from temporal (periodic) noise which is related to circadian oscillation [16]. In accordance with such experimental observations, theoretical studies also conclude that biochemical noise is not Gaussian to facilitate enhanced functionality [17, 18]. Both experimental and theoretical approaches suggest fundamental roles of noise-enhanced phenomena to render efficient molecular systems.

In this paper, we investigate the efficiency of *Brownian motor* [19, 20] (or a ratchet transport) under a noisy, nonequilibrium state. It is known that the violation of detailed balance induces a transport effect, which is a model for many biological mechanisms including ion pumps [21–23] that use ATP for transport (In theory, however, the conformational fluctuation of such pumps can facilitate transport even without ATP [24]).

Brownian transport has been intensively studied including in mass separation [25], electron transport in a quantum ratchet [26], transport of atoms in optical traps [27], a random walker model [28], and non-Gaussian noise models [29, 30] (for more details, see comprehensive reviews [20, 31]). One of the most popular ratchet models is the correlation ratchet in which Brownian particles in a ratchet potential are driven by the **addition** of white and colored noise. The model studied here is a ratchet driven by the **multiplication** of white and colored noise. Let us introduce our model more formally.

Superstatistics with temporal and/or spatial fluctuations [32–35] is used to explain non-Gaussian distributions [36, 37] in applied physics. This concept is also seen in stochastic

processes in which noise fluctuation is treated in a static way [33, 38–43]. The superstatistical stochastic process calculates a stationary distribution $P_{st}(x)$ by assuming that the noise fluctuates over a long time scale (i.e., very slowly):

$$P_{st}(x) = \int_0^\infty dD\, P_{st}(x|D)P(D), \tag{1}$$

where $P_{st}(x|D)$ is the stationary distribution given the noise intensity D and $P(D)$ is the distribution of D. Equation 1 fits in the Bayesian framework by considering $P_{st}(x)$ and $P(D)$ as posterior and prior distributions, respectively.

We model temporal noise-intensity fluctuation dynamically and modulated the intensity of white Gaussian noise by the Ornstein–Uhlenbeck process in overdamped Langevin equations [44, 45]:

$$\dot{x} = -V'(x) + s\xi_x(t), \tag{2}$$

$$\dot{s} = -\gamma(s-\alpha) + \sqrt{\gamma}\xi_s(t). \tag{3}$$

Here, $V(x)$ is the potential, α is the mean of the Ornstein–Uhlenbeck process, γ is the relaxation rate ($\gamma > 0$), and $\xi_x(t)$ and $\xi_s(t)$ are white Gaussian noise with the correlation:

$$\langle \xi_x(t)\xi_x(t')\rangle = 2D_x\delta(t-t'), \tag{4}$$

$$\langle \xi_s(t)\xi_s(t')\rangle = 2D_s\delta(t-t'). \tag{5}$$

We call the term $s(t)\xi_x(t)$, the *stochastic intensity noise* (SIN) because the noise intensity is governed by a stochastic process. SIN is the multiplicative term of white and colored noise, and qualitatively different from white noise: it is in nonequilibrium.

In the context of Brownian transport, Reimann *et al.* [46] first studied the transport effect with sinusoidal noise-intensity modulation. Our work differs from this and succeeding studies that employed a discrete dichotomous noise or a deterministic periodic signal [46–48]; in our model, fluctuations are governed by a continuous stochastic process (the Ornstein–Uhlenbeck process). There exist similar models. Borromeo *et al.* studied a current generated by two symmetric colored noises, the Ornstein–Uhlenbeck noise and its time-delayed version, and observed the Maxwell's daemon-like phenomenon [49]. Morgado *et al.* investigated temporal heterogeneity in Poisson mechanism [50]. Our model focuses on a multiplicative rather than an additive effect, because biological phenomena are governed by multiplication (also see Discussion). This distinction highlights the importance of SIN-induced transport.

In our calculations, we investigated the effect of four controllable parameters on the current:

- γ (the relaxation rate in Equation 7),
- Q (the effective noise intensity in Equation 11),
- ρ (the squared variation coefficient in Equation 12) and
- μ (the scaled mass in Equation 6).

Although D_x (the noise-intensity in Equation 6) is also a controllable parameter, we kept it constant ($D_x = 1$) throughout the paper. The squared variation coefficient ρ, which is generally defined as the ratio of the squared mean to the variance, characterizes the deviation of the Gaussian noise distribution by the kurtosis. The overdamped case is calculated using the matrix continued fraction method (MCFM) and Monte Carlo (MC) simulations. The calculations reveal that the current is a maximum at adequate γ and Q. This result concurs with resonant activation (RA) [51] and noise-enhanced stability (NES) [52, 53] in the escape problem. Our main result is the enhanced transport capability in intermediate time-correlation regions. This has an important biological implication. The time-correlation of extrinsic noise (i.e., environmental fluctuation) with gene expression in *E. coli* is on the order of cell cycle length [54]. By fitting the time-scale of our model to the *E. coli* model in Ref. [55], we found that the time-correlation of extrinsic noise coincides with the region of enhanced transport. It is a theoretical backup of the tactful exploitation of environmental fluctuation by biological organisms.

2. METHODS

2.1. Brownian Particles

Brownian particles are subject to noise-intensity fluctuations represented by

$$\mu\ddot{x} = -\dot{x} - V'(x) + s\xi_x(t), \tag{6}$$

$$\dot{s} = -\gamma(s - \alpha) + \sqrt{\gamma}\xi_s(t), \tag{7}$$

where the scaled mass μ is introduced into Equation 2 for a study of a mass separation effect, and meanings of $V(x)$ are the same as in Equation 2. We used the same ratchet potential

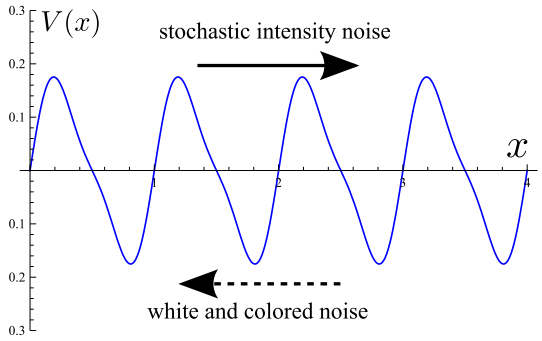

FIG. 1: (Online version in color) A ratchet potential of Equation 8. The dashed and solid arrows indicate the directions of the current in the correlation ratchet (driven by additive white and colored noise) and the ratchet (driven by SIN), respectively.

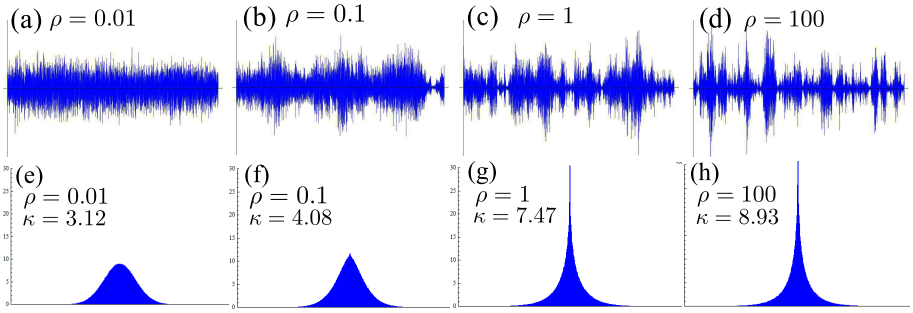

FIG. 2: (Online version in color) (a)–(d) Time courses of SIN generated by MC simulations for four values of ρ (squared variation coefficient given by Equation 12): $\rho =$ (a) 0.01, (b) 0.1, (c) 1, and (d) 100. (e)–(h) Histograms of SIN for the four values of ρ and their sample kurtosis κ. In (a)–(h), we varied ρ while keeping the effective intensity $Q = D_x(D_s + \alpha^2)$ constant.

function as used in previous studies [56, 57]

$$V(x) = \frac{1}{2\pi}\left\{\sin(2\pi x) + \frac{1}{4}\sin(4\pi x)\right\} + Fx, \tag{8}$$

with a periodicity $V(x+1) = V(x)$ $(F = 0)$, where F is the load. Figure 1 shows the potential with no load $(F = 0)$, where the dashed and solid arrows indicate the normal current direction for the correlation ratchet [56, 57] and for the ratchet driven by SIN, respectively. The current direction for the SIN case is identical to that in Ref. [47] in which the noise intensity is modulated by a random dichotomous process. In Equation 7, the relaxation rate γ denotes the inverse of a time scale (time-correlation). When the noise intensity fluctuates with a longer time scale $(\gamma \to 0)$, systems driven by SIN locally equilibrates and hence a

current is not generated in accordance with the second law of thermodynamics. Likewise, SIN reduces to white noise (with a noise intensity Q) when the noise-intensity fluctuates very rapidly ($\gamma \to \infty$) [44], which also indicates that the current vanishes.

For Equation 7, the stationary distribution $P_{st}(s)$ of the intensity-modulation term s is given by

$$P_{st}(s) = \frac{1}{\sqrt{2\pi D_s}} \exp\left\{-\frac{1}{2D_s}(s-\alpha)^2\right\}. \tag{9}$$

A calculation of the correlation function of SIN yields [45]

$$\langle s(t)\xi_x(t)s(t')\xi_x(t')\rangle = 2Q\delta(t-t'), \tag{10}$$

with

$$Q = D_x(D_s + \alpha^2), \tag{11}$$

where Q expresses the effective noise intensity and D_x and D_s are the noise intensities of $\xi_x(t)$ and $\xi_s(t)$, respectively [Equations 4 and 5]. Here, we introduce the squared variation coefficient ρ of the noise-intensity fluctuations [45]:

$$\rho = D_s/\alpha^2, \tag{12}$$

which denotes the squared ratio of the standard deviation to the mean of Equation 9. Figures 2(a)–(d) show trajectories of SIN with $\rho = 0.01$, 0.1, 1, and 100, respectively. All share the same effective noise intensity Q (the same variance). For $\rho = 0$, SIN reduces to white Gaussian noise with a noise intensity $Q = D_x\alpha^2$. On increasing ρ (Figures 2(e)–(h)), the noise-intensity fluctuations become larger and the distribution of SIN deviates from the Gaussian distribution. To quantify the deviation, we calculate the kurtosis of SIN, which is a measure of heavy tails in probability density functions. The kurtosis κ of SIN (i.e., $s(t)\xi_x(t)$) is given by (Appendix A)

$$\kappa = \frac{\left\langle \{s(t)\xi_x(t)\}^4 \right\rangle}{\left\langle \{s(t)\xi_x(t)\}^2 \right\rangle^2} = 9 - \frac{6}{(1+\rho)^2} \quad (0 \le \rho < \infty), \tag{13}$$

where κ depends only on the squared variation coefficient ρ having a crucial effect on the statistical properties of SIN. Equation 13 shows that the kurtosis is 3 for $\rho = 0$ and κ increases with increasing ρ, giving a flatter distribution. Equation 13 is plotted by the solid curve in Figure 3 in which the filled circles denote the kurtosis calculated by MC simulations.

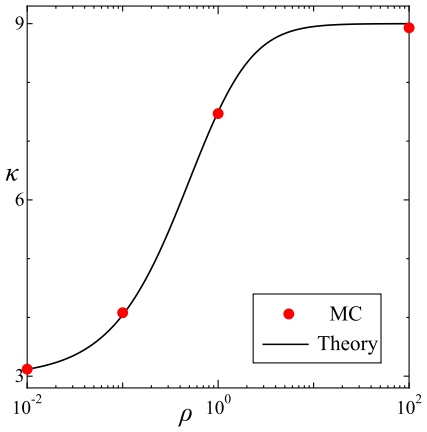

FIG. 3: (Online version in color) Kurtosis κ of SIN as a function of ρ. The solid line indicates Equation 13 and the filled circles indicate the sample kurtosis in Figures 2(e)–(h).

3. RESULTS

In Equations 6 and 7, our model has four parameters (γ, α, D_x, and D_s) in terms of noise properties. Instead of these parameters, we adopt γ, ρ (the squared variation coefficient in Equation 12), Q (the effective noise intensity in Equation 11), and D_x as controllable parameters in model calculations, where Q and ρ are defined by Equations 11 and 12, respectively. The new parameters (γ, ρ, Q, and D_x) specify the system identically since α and D_s are uniquely determined by D_x, Q, and ρ:

$$\alpha = \sqrt{\frac{Q}{D_x(1+\rho)}}, \quad D_s = \frac{\rho Q}{D_x(1+\rho)}. \tag{14}$$

Performing model calculations based on the MCFM and MC simulations, we studied the dependence of the current on γ, ρ, and Q in the overdamped case (D_x is set to $D_x = 1$ throughout the paper). In the underdamped case, we additionally investigated the dependence of the current on the scaled mass μ (Equation 6) with MC simulations. MC simulations were performed with the Euler-forward method with a time resolution of $\Delta t = 10^{-4}$ (for details of the method, see Ref. [58]).

3.1. Overdamped case

We first calculated the current J for the overdamped case ($\mu = 0$ in Equation 6). For $t \to \infty$, the stationary distribution $P_{st}(x, s)$ of (x, s) has to satisfy the stationary Fokker–

Planck equation (FPE)

$$\mathbb{L}_{\mathrm{FP}} P_{st}(x,s) = 0, \tag{15}$$

where $\mathbb{L}_{\mathrm{FP}}$ is an FPE operator:

$$\mathbb{L}_{\mathrm{FP}} = \frac{\partial}{\partial x} V'(x) + D_x \frac{\partial^2}{\partial x^2} s^2 + \gamma \left\{ \frac{\partial}{\partial s}(s-\alpha) + D_s \frac{\partial^2}{\partial s^2} \right\}. \tag{16}$$

Since Equation 15 is not written in terms of potential forms, we cannot calculate the stationary distribution in a closed form. Consequently, we used the MCFM to solve Equation 15, which expands $P_{st}(x,s)$ in terms of a complete orthonormal set. The MCFM is a common technique for stochastic processes and it is widely used to solve FPEs (see Ref. [58] and references therein). Considering the periodicity of the potential $[V'(x+1) = V'(x)]$ and domain $[x \in (-\infty, \infty)$ and $s \in (-\infty, \infty)]$, we expanded the stationary distribution $P_{st}(x,s)$ in a Fourier series for x and the Hermite function for s:

$$P_{st}(x,s) = \psi_0(s) \sum_{k=-M_k}^{M_k} \sum_{n=0}^{M_n} C_{k,n} \exp\left(2\pi k \mathrm{i} x\right) \psi_n(s). \tag{17}$$

Here, $C_{k,n}$ are expansion coefficients, M_k and M_n are truncation numbers on which the precision of obtained solutions depends, and $\psi_n(s)$ is the Hermite function satisfying the orthonormality relation $\langle \psi_{n'}(s) \psi_n(s) \rangle = \delta_{n'n}$:

$$\psi_n(s) \;=\; \left(\frac{1}{2\pi D_s}\right)^{1/4} \sqrt{\frac{1}{2^n n!}} H_n(\eta) \exp\left(-\frac{1}{2}\eta^2\right) \quad \eta = \sqrt{\frac{1}{2D_s}}(s-\alpha), \tag{18}$$

where $H_n(s)$ is the nth Hermite polynomial. Multiplying Equation 15 by $\exp(-2\pi k' \mathrm{i} x)\psi_{n'}(s)/\psi_0(s)$ and integrating over x and s, we obtain a linear algebraic equation in terms of $C_{k,n}$, which can be solved by the MCFM (Appendix B). The current J is calculated using

$$J = \langle v \rangle = \int_0^1 dx \left(\int_{-\infty}^{\infty} ds\, J_x(x,s) \right), \tag{19}$$

where $J_x(x,s)$ is the probability current in the x direction due to the continuity equation $\partial_t P + \partial_x J_x + \partial_s J_s = 0$:

$$J_x(x,s) = \left(-V'(x) - D_x s^2 \frac{\partial}{\partial x} \right) P_{st}(x,s). \tag{20}$$

By substituting Equation 17 into Equation 19, the current J can be expressed in terms of $C_{k,n}$:

$$J = -\frac{1}{2}(C_{-1,0} + C_{1,0}) - \frac{1}{4}\left(C_{-2,0} + C_{2,0}\right) - F C_{0,0}. \tag{21}$$

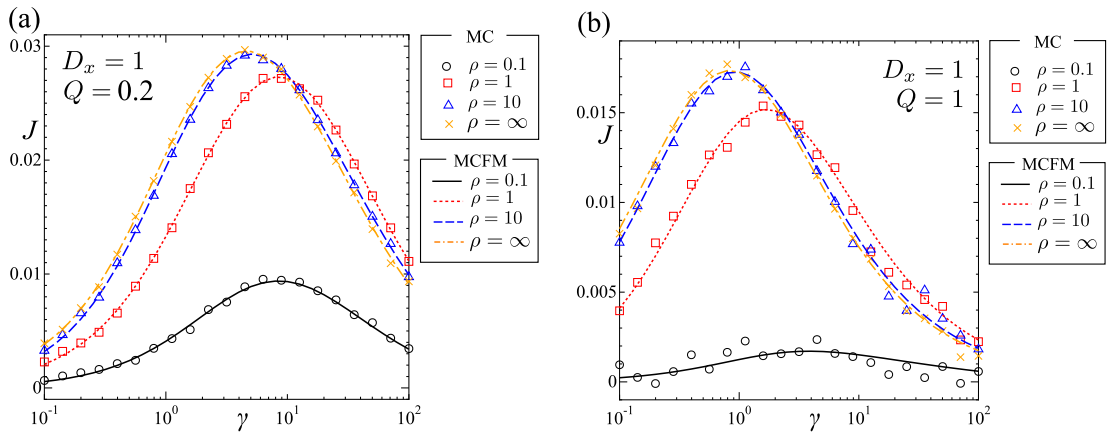

FIG. 4: (Online version in color) Current J as a function γ for the overdamped case ($\mu = 0$). The lines and symbols represent J calculated using the MCFM and MC simulations, respectively. The parameters are (a) $D_x = 1$ and $Q = 0.2$ and (b) $D_x = 1$ and $Q = 1$, with $\rho = 0.1$ (solid lines and circles), $\rho = 1$ (dotted lines and squares), $\rho = 10$ (dashed lines and triangles), and $\rho = \infty$ (dot-dashed lines and crosses).

The current given by Equation 21 does not vanish even when there is no load (i.e. $F = 0$) due to the broken detailed balance.

In practical calculations of Equation 21, we increased the truncation numbers M_k and M_n in Equation 17 until the current J converged. We also performed MC simulations to verify reliability of the MCFM, where the velocity is given by $v = [x(T) - x(0)]/T$ ($T = 10^5$). The calculation was repeated 100 times and the average velocity was determined. Below, we calculate the dependence of the current J on the relaxation rate γ (Figure 4), the effective noise intensity Q (Figure 5), and the squared variation coefficient ρ (Figure 6).

We first show the current J as a function of the relaxation rate γ [Equation 3]. In Figure 4, γ is plotted against the current J for two sets of parameters: Case (a) $D_x = 1$ and $Q = 0.2$ (Figure 4(a)), and Case (b) $D_x = 1$ and $Q = 1$ (Figure 4(b)). The relationship was computed for four values of ρ (the squared variation coefficient): $\rho = 0.1, 1, 10$, and ∞ (the case $\rho = \infty$ corresponds to $\alpha = 0$ and $D_s = Q/D_x$). In Case (a), J became a maximum at an intermediate γ, while the current vanished for both $\gamma \to 0$ and $\gamma \to \infty$. The small current at $\rho = 0.1$ was expected because a small ρ corresponds to weak noise fluctuations. Because larger ρ means larger fluctuations (the kurtosis monotonically increases as a function of ρ, as shown in Figure 3), it is natural that the current increases as ρ increases. However, J in

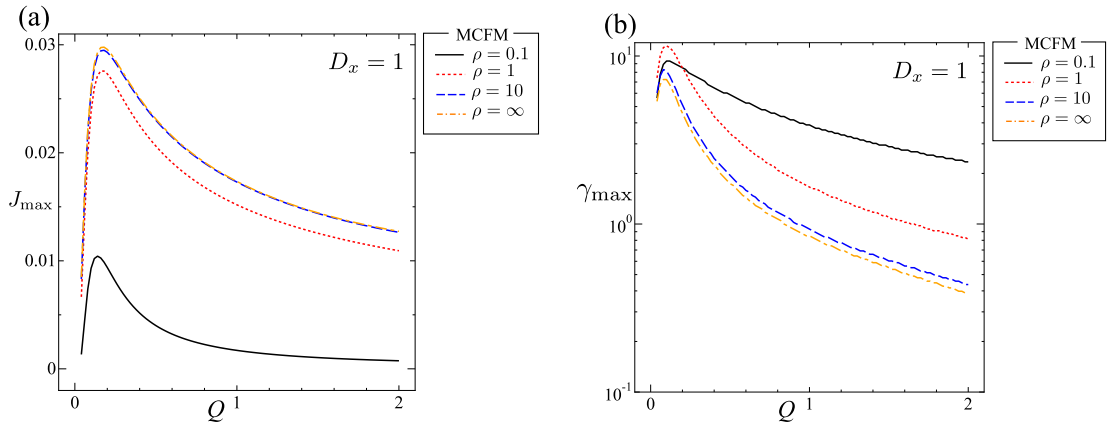

FIG. 5: (Online version in color) (a) Current $J_{\max}$ and (b) $\gamma_{\max}$ as a function Q for the overdamped case ($\mu = 0$). The parameters are $D_x = 1$ with $\rho = 0.1$ (solid lines), $\rho = 1$ (dotted lines), $\rho = 10$ (dashed lines), and $\rho = \infty$ (dot-dashed lines).

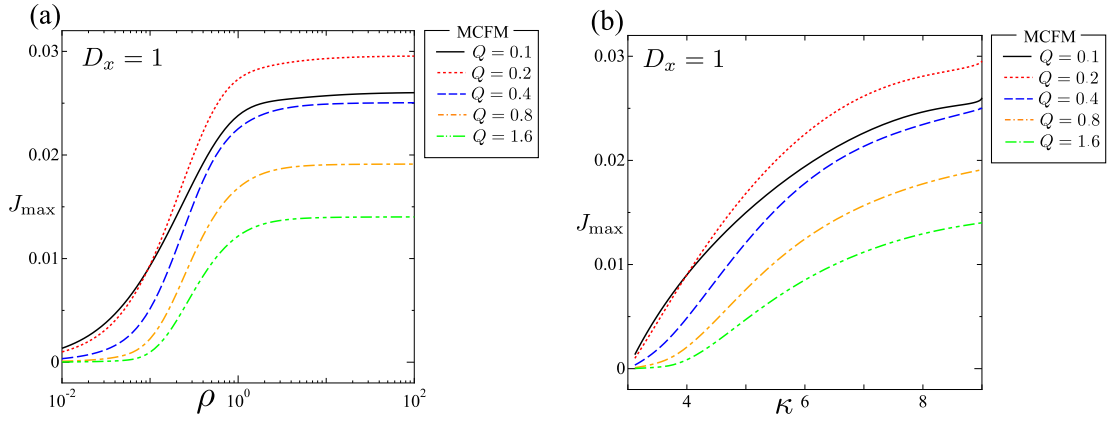

FIG. 6: (Online version in color) $J_{\max}$ as a function of (a) squared variation coefficient ρ and (b) kurtosis κ for the overdamped case ($\mu = 0$). The parameters are $D_x = 1$ with $Q = 0.1$ (solid lines), $Q = 0.2$ (dotted lines), $Q = 0.4$ (dashed lines), $Q = 0.8$ (dot-dashed lines), and $Q = 1.6$ (dot-dot-dashed lines).

the range $\gamma > 10$ shows a different tendency and it is higher when $\rho = 1$ than when $\rho = 10$ or $\rho = \infty$. This is due to the noise-intensity modeling in Equation 7; specifically, $s(t)$ in Equation 7 for small ρ rarely has negative values, whereas $s(t)$ for large ρ has negative as well as positive values. For large γ cases, the "effective" relaxation rate might be measured by $\langle |s(t)||s(t')| \rangle$ rather than by $\langle s(t)s(t') \rangle$, which indicates that the effective relaxation rates for larger ρ cases are larger than their actual values. In Figure 4, the results obtained by the MCFM (lines) are always in agreement with MC simulations (symbols), which indicates

the reliability of the MCFM. The MC simulations tended to converge for smaller Q cases because v is more centered on the mean (thin distributions) when the effective noise intensity is smaller. We also note the difference between our model and that of Ref. [46] where noise-intensity is modulated by a deterministic sinusoidal signal. We found that the width of peaks tends to be wider in our model, which is a consequence that the power spectrum of Ornstein–Uhlenbeck noise have the Lorentzian function whereas that of a sinusoidal function is a delta-peaked function.

We next show the current J as a function of the effective noise intensity Q [Equation 11]. Since the effect of the relaxation rate γ varies depending on the squared variation coefficient ρ (as shown above), we removed the γ dependence of the current J by taking the maximum in terms of γ:

$$J_{\max} = J_{\max}(D_x, Q, \rho) \;=\; \max_{\gamma} J(D_x, \gamma, Q, \rho), \tag{22}$$

$$\gamma_{\max} = \gamma_{\max}(D_x, Q, \rho) \;=\; \operatorname*{argmax}_{\gamma} J(D_x, \gamma, Q, \rho). \tag{23}$$

Here, $J_{\max}$ and $\gamma_{\max}$ respectively denote the maximum current and γ when the current is a maximum. Figures 5(a) and (b) show plots of Q against $J_{\max}$ and $\gamma_{\max}$ for $D_x = 1$, respectively. Again, computations were performed for four values of ρ. In Figure 5(a), $J_{\max}$ has maxima as a function Q; the magnitude of this maxima is small for $\rho = 0.1$, as in Figure 4. Transport effects are robust in terms of the noise intensity Q, because the current for $Q = 2$ still exhibits half the maximum current (around $Q = 0.2$) for large ρ cases. Figure 5(b) shows $\gamma_{\max}$ (i.e., the relaxation rate yielding the maximum current) as a function of Q. For all four values of ρ, $\gamma_{\max}$ has a maximum value around $Q = 0.1$ and decreases with increasing Q. This result shows that the noise intensity has to fluctuate over a long time scale to enhance the transport capability in noisy environments.

We also investigated the dependence of ρ on $J_{\max}$ while keeping the other parameters constant. Figure 6(a) shows $J_{\max}$ (Equation 22) as a function of ρ with $D_x = 1$ and five values of Q (the effective noise intensity): $Q = 0.1, 0.2, 0.4, 0.8$, and 1.6. $J_{\max}$ increases monotonically; the increase exhibits sigmoid-like behavior in terms of $\log \rho$, indicating that $J_{\max}$ is an extremely nonlinear function in terms of ρ. Figure 6(b) shows the dependence of $J_{\max}$ on the kurtosis κ (Equation 13). Although $J_{\max}$ still exhibits nonlinearity as a function of κ, its nonlinearity is much smaller than that of ρ. This result shows that the kurtosis can be used as an index parameter for Brownian transport driven by noise-intensity fluctuations.

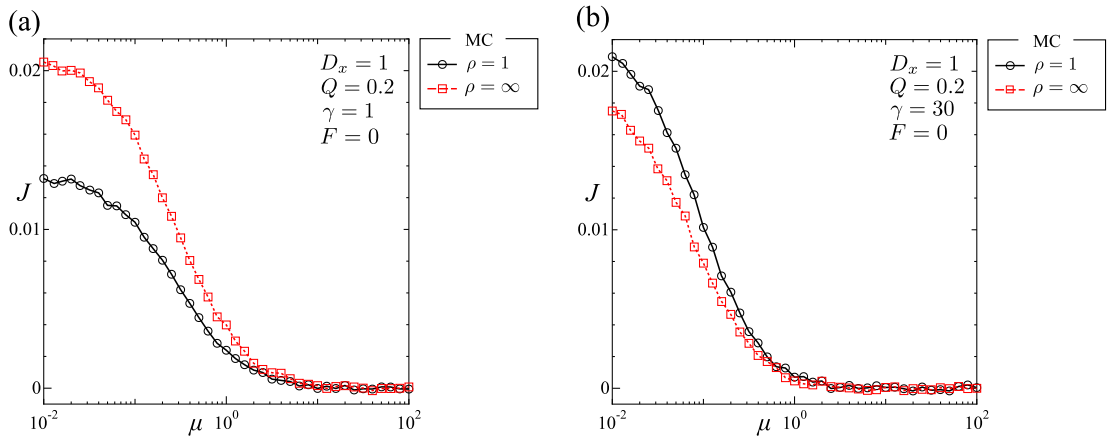

FIG. 7: (Online version in color) Current J as a function of μ using MC simulations for (a) $\gamma = 1$ and (b) $\gamma = 30$. The other parameters are $D_x = 1$, $Q = 0.2$, and $F = 0$ with $\rho = 1$ (circles) and $\rho = \infty$ (squares). Lines are included as a guide to the eye only.

3.2. Underdamped case

We next investigated Brownian transport (Equations 6 and 7) in the underdamped regime, especially from the viewpoint of a mass separation effect [25]. Although we could use the MCFM for the overdamped case, the MCFM for an underdamped FPE did not yield stable solutions in terms of the current (data not shown) so that we used MC simulations only. The underdamped model includes an extra parameter μ (scaled mass) in addition to the four parameters (γ, ρ, Q, and D_x). The velocity is given by $v = [x(T) - x(0)]/T$ ($T = 10^5$). The calculation was repeated 100 times to obtain the current as the average velocity.

We first show the current J as a function of the scaled mass μ. Figure 7 shows the dependence of the current J on μ for two values of γ [Case (a) $\gamma = 1$ (Figure 7(a)) and Case (b) $\gamma = 30$ (Figure 7(b))], where the other parameters are $D_x = 1$, $Q = 0.2$, $F = 0$, and $\rho = 1$ (circles) or $\rho = \infty$ (squares). In Case (a), the current decreases monotonically and the current for $\rho = \infty$ always exceeds that for $\rho = 1$. In contrast, in Case (b), the current of $\rho = \infty$ is always smaller than that of $\rho = 1$ and the relation between the magnitudes for $\rho = 1$ and $\rho = \infty$ differs from that for Case (a). As shown in Figure 5, the "effective" relaxation rate for larger ρ is larger than the actual relaxation rate. This is the reason why converse magnitude relaxation occurs between $\rho = 1$ and $\rho = \infty$ in Case (b).

We next show the dependence of the average current J on γ for two values of Q (the

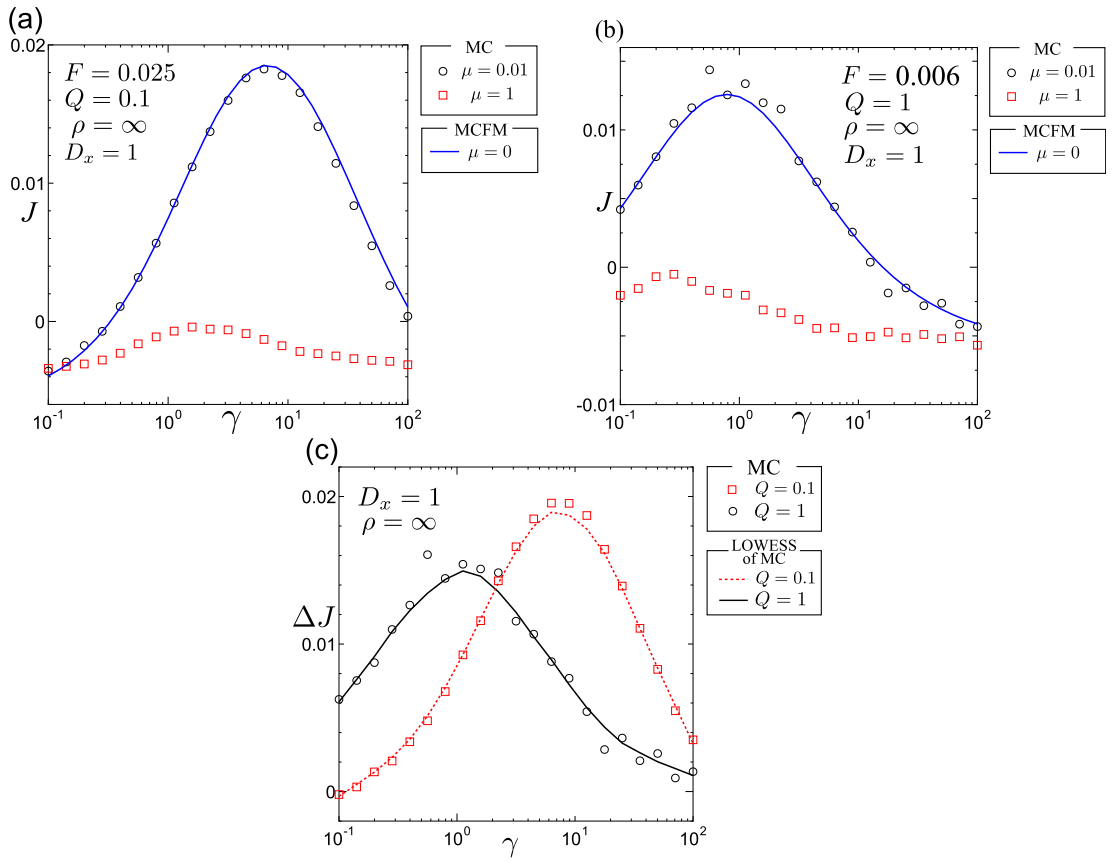

FIG. 8: (Online version in color) (a) and (b) Current J with load $F > 0$ as a function of γ using MC simulations for (a) $D_x = 1$, $Q = 0.1$, $\rho = \infty$, and $F = 0.025$; and (b) $D_x = 1$, $Q = 1$, $\rho = \infty$ and $F = 0.006$. J is calculated with MC simulations with $\mu = 0.01$ (circles) and $\mu = 1$ (squares), and the overdamped case ($\mu = 0$) is also shown (solid line). (c) ΔJ (difference of the currents for $\mu = 0.01$ and 1 defined by Equation 24) as a function γ for two mass separations. Lines represent LOWESS (locally weighted scatterplot smoothing) of MC simulations (see the text).

effective noise intensity): Case (a) $Q = 0.1$ [$D_x = 1$, $\rho = \infty$, and $F = 0.025$] (Figure 8(a)) and Case (b) $Q = 1$ [$D_x = 1$, $\rho = \infty$, and $F = 0.006$] (Figure 8(b)). In both cases, the load F [Case (a) $F = 0.025$ and Case (b) $F = 0.006$] increased the ratchet potential for larger values of x and the value of F was determined such that particles of $\mu = 0.01$ and $\mu = 1$ move in opposite directions. Figure 8 shows J of $\mu = 0.01$ (circles) and $\mu = 1$ (squares) for $Q = 0.1$ (Figure 8(a)) and $Q = 1$ (Figure 8(b)), where the lines show the MCFM results for the overdamped case ($\mu = 0$). We include the $\mu = 0.01$ case along with the MCFM result to show that results of the underdamped case decrease asymptotically to the overdamped case as $\mu \to 0$. In Cases (a) and (b), the current J for $\mu = 0.01$ has positive values, unlike J for

$\mu = 1$, which is negative over the whole range of γ. J for $\mu = 0.01$ has peaks at intermediate γ values; however, the $\gamma_{\max}$ values at which the current is a maximum are different in Cases (a) and (b): $\gamma_{\max}$ in Case (a) ($Q = 0.1$) is around 10, whereas $\gamma_{\max}$ in Case (b) ($Q = 1$) is about 1. Since the currents for $\mu = 0.01$ and $\mu = 1$ move in the opposite directions, particles with $\mu = 0.01$ and $\mu = 1$ can be set apart due to the mass separation effect. To quantify the mass separation capability, we define ΔJ as

$$\Delta J = J(\mu = 0.01) - J(\mu = 1). \tag{24}$$

ΔJ is a quantity of interest for the separation phenomenon, and systems with larger ΔJ exhibit a better separation capability. Figure 8(c) shows ΔJ for two cases [Case (a) ($Q = 0.1$) and Case (b) ($Q = 1$)] and the lines show locally weighted scatterplot smoothing (LOWESS) for each data. It clearly shows that γ at which the mass separation capability is a maximum is different for the two Q cases and that better mass separation is realized at smaller γ values in the larger Q case. This result shows that the mass separation capability is greater for slower environmental fluctuations when Brownian motors are subject to strong noise.

4. DISCUSSION

We investigated the statistical properties of SIN on Brownian ratchet and found that the current was enhanced for smaller γ in both the overdamped and underdamped regimes (Figures 5 and 8) when the effective noise-intensity Q is larger. This result is intriguing because a smaller γ corresponds to extrinsic fluctuations with a larger time scale. In single-cell experiments on *E. coli*, assuming that mRNA production is Poissonian and that the protein burst size has an exponential distribution, the protein copy number obeys the gamma distribution [15]:

$$P(x) = \frac{x^{a-1}e^{-x/b}}{\Gamma(a)b^a}, \tag{25}$$

where a and b are parameters. Observations [15] revealed that the fluctuations (extrinsic noise) in a and b are slow and the stationary distribution can be approximated as

$$P(x) = \int_0^\infty db \int_0^\infty da \, \frac{x^{a-1}e^{-x/b}}{\Gamma(a)b^a} P(a)P(b), \tag{26}$$

where $P(a)$ and $P(b)$ denote the distributions of a and b, respectively. Note that Equation 26 is equivalent to the description of superstatistics (see Equation 1). In stochastic

gene expression, the intrinsic noise is rather well-explained: its source is stochastic chemical reactions with small number of molecules. In contrast, contribution of the extrinsic noise has not been well reasoned or modeled [59, 60]. Stochastic gene expression is often modeled with Langevin equations, i.e., continuous approximation of the continuous-time Markov chain through Van Kampen's expansion [61]. Many models assume that extrinsic noise affect the transcriptional, translational and degradation kinetics as in Equation 26, which results in both drift terms and noise-intensity fluctuations of corresponding Langevin equations. The stochastic term of Langevin equations is often approximated with the additive white noise, and therefore, the extrinsic noise-induced fluctuation fits the overdamped case given by Equation 6 and 7, assuming that the drift term fluctuation is negligible compared to that of the noise-intensity. Our calculations showed that environmental fluctuations should be slow to enhance the transport capability in noisy environments. That is, fluctuations in a and b in Equation 25 occur over long time scales.

Lastly, let us show the correspondence of our calculations with actual time-scales in biological experiments. Refs. [54] observed that the time correlation of extrinsic fluctuations in *E. coli* is in the order of cell cycle length T_{cc}. The deterministic part of the protein concentration x generally obeys

$$\frac{dx}{dt} = f_+ - \beta x, \tag{27}$$

where f_+ is a protein synthesis term (via translation) and β is the degradation rate. In Langevin equations, the degradation rate corresponds to the relaxation rate (reciprocal of relaxation time) and hence it determines the time scale. Dunlop *et al.* [55] defined $\beta = \log 2/T_{cc}$ and concluded that the time correlation of the extrinsic fluctuation is $\tau = T_{cc}/\log 2$ ($T_{cc} = 60\,\mathrm{min}$). Because the ratchet potential given by Equation 8 can be approximated by a quadratic function around the minima, Equation 6 can be cast in the form of Equation 27 with $\beta \simeq 10$. Matching the time scales of these two systems by comparing the relaxation time (i.e., comparing β in the two cases), the time correlation of the extrinsic fluctuations observed in *E. coli* corresponds to $\tau = 0.1$ in our ratchet potential model. Figure 5 shows that $\gamma_{\max}$ is in the approximate range of 1–10, which implies that $\tau_{\max} = \gamma_{\max}^{-1} = 0.1 \sim 1$. Therefore, the extrinsic noise in the experimental observation is close to optimal for the transport effect. Extrinsic noise has non-negligible time-correlation, leaving the system at nonequilibrium states. Although there remains a biochemical gap between gene expressions and ion transports, our result shows the biochemical advantage of exploiting extrinsic noise

for gene regulation.

In summary, we investigated the transport properties of Brownian ratchet in both overdamped and underdamped regimes [44, 45]. In the overdamped regime, our calculations by the MCFM and MC simulations revealed the existence of a maximum current as a function of γ (the relaxation rate) and Q (the effective noise intensity). The maximum current is induced at a lower relaxation rate γ for higher noise intensities. In the underdamped regime, MC calculations also showed a maximum for smaller γ when systems are subject to noisy environments. Consequently, the mass separation capability was also maximized for smaller γ in such cases. We continue the investigation of ratchet transport in specific biological models in future studies.

Acknowledgments

This work was supported by a Global COE program "Deciphering Biosphere from Genome Big Bang" from the Ministry of Education, Culture, Sports, Science and Technology (MEXT), Japan (YH) and a Grant-in-Aid for Young Scientists B (#23700263) from MEXT, Japan (YH).

Appendix A: Kurtosis of SIN

We calculate kurtosis κ of SIN defined by

$$\kappa = \frac{\left\langle \left\{ s(t)\xi_x(t) \right\}^4 \right\rangle}{\left\langle \left\{ s(t)\xi_x(t) \right\}^2 \right\rangle^2}. \tag{A1}$$

By using an independence relation between s and ξ_x and the Gaussian nature of ξ_x, the numerator and denominator in Equation A1 are given by

$$\left\langle \left\{ s(t)\xi_x(t) \right\}^4 \right\rangle = 3 \left\langle s(t)^4 \right\rangle \left\langle \xi_x(t)^2 \right\rangle^2, \tag{A2}$$

$$\left\langle \left\{ s(t)\xi_x(t) \right\}^2 \right\rangle^2 = \left\langle s(t)^2 \right\rangle^2 \left\langle \xi_x(t)^2 \right\rangle^2. \tag{A3}$$

Let $u(t) = s(t) - \alpha$. Since $u(t)$ is a standard Ornstein–Uhlenbeck process with $\langle u(t) \rangle = 0$, the second and fourth-order moments are $\langle u(t)^2 \rangle = D_s$ and $\langle u(t)^4 \rangle = 3D_s^2$, which yields

$$\left\langle s(t)^2 \right\rangle = \left\langle u(t)^2 \right\rangle + \alpha^2 = D_s + \alpha^2, \tag{A4}$$

$$\left\langle s(t)^4 \right\rangle = \alpha^4 + 6\alpha^2 \left\langle u(t)^2 \right\rangle + \left\langle u(t)^4 \right\rangle = \alpha^4 + 6\alpha^2 D_s + 3D_s^2. \tag{A5}$$

With Equations A2–A5, the kurtosis is calculated into

$$\kappa = \frac{3\left(\alpha^4 + 6\alpha^2 D_s + 3D_s^2\right)}{\left(D_s + \alpha^2\right)^2}. \tag{A6}$$

Substituting $\rho = D_s/\alpha^2$ into Equation A6, we obtain Equation 13.

Appendix B: Matrix continued fraction method

We explain the procedure of the MCFM in the overdamped case. Substituting Equation 17 into Equation 15, we obtain a linear algebraic equation:

$$\begin{aligned} 0 \;=\; & C_{k,n}\left[-n\gamma + 2F\pi k\mathrm{i} - 4\pi^2 D_x k^2\left\{\alpha^2 + 2D_s\left(n+\frac{1}{2}\right)\right\}\right] \\ & + C_{k-1,n}\pi k\mathrm{i} + C_{k+1,n}\pi k\mathrm{i} + \frac{C_{k-2,n}}{2}\pi k\mathrm{i} + \frac{C_{k+2,n}}{2}\pi k\mathrm{i} \\ & - 4C_{k,n+2}\pi^2 D_x D_s k^2\sqrt{(n+2)(n+1)} - 4C_{k,n-2}\pi^2 D_x D_s k^2\sqrt{n(n-1)} \\ & - 8C_{k,n-1}\pi^2 D_x \alpha k^2\sqrt{D_s n} - 8C_{k,n+1}\pi^2 D_x \alpha k^2\sqrt{D_s(n+1)}, \end{aligned} \tag{B1}$$

where the dimension of the linear algebraic equation (B1) is $(2M_k+1)(M_n+1)$. We show the procedure of the MCFM, since a naive conversion of Equation B1 yields an equation with second-nearest-neighbor coupling, which is not compatible with the MCFM (the MCFM can treat only first-nearest-neighbor coupling). By introducing $c_k = (C_{k,0}, C_{k,1}\cdots, C_{k,M_n})^{\mathsf{T}}$, Equation B1 is calculated into

$$0 = \frac{\pi k\mathrm{i}\mathsf{E}c_{k-2}}{2} + \pi k\mathrm{i}\mathsf{E}c_{k-1} + \left[\mathsf{A} - 4\pi^2 D_x k^2\mathsf{B} + 2F\pi k\mathrm{i}\mathsf{E}\right]c_k + \pi k\mathrm{i}\mathsf{E}c_{k+1} + \frac{\pi k\mathrm{i}\mathsf{E}c_{k+2}}{2}. \tag{B2}$$

Here, E is the identity matrix and A and B are $(M_n+1)\times(M_n+1)$ matrices defined by

$$\mathsf{A}_{n+1,n'+1} \;=\; -n\gamma\delta_{n,n'}, \tag{B3}$$

$$\begin{aligned} \mathsf{B}_{n+1,n'+1} \;=\; & \left\{\alpha^2 + 2D_s\left(n+\frac{1}{2}\right)\right\}\delta_{n,n'} + 2\alpha\sqrt{D_s n}\,\delta_{n-1,n'} + 2\alpha\sqrt{D_s(n+1)}\,\delta_{n+1,n'}, \\ & + D_s\sqrt{n(n-1)}\,\delta_{n-2,n'} + D_s\sqrt{(n+1)(n+2)}\,\delta_{n+2,n'}, \end{aligned} \tag{B4}$$

where $0 \le n \le M_n$ and $0 \le n' \le M_n$. Introducing $\tilde{c}_k = (c_{2k}^{\mathsf{T}}, c_{2k+1}^{\mathsf{T}})^{\mathsf{T}}$ [58], Equation B2, which is an equation with second-nearest-neighbor coupling, reduces to the following equation with first-nearest-neighbor coupling:

$$0 = \mathsf{Q}_k^{-}\tilde{c}_{k-1} + \mathsf{Q}_k\tilde{c}_k + \mathsf{Q}_k^{+}\tilde{c}_{k+1}, \tag{B5}$$

where Q_k are $(2M_n+2)\times(2M_n+2)$ matrices consisting of submatrices A and B:

$$\mathsf{Q}_k^- = \begin{pmatrix} \pi k\mathrm{i}\mathsf{E} & 2\pi k\mathrm{i}\mathsf{E} \\ \mathsf{0} & \pi(2k+1)\mathrm{i}\mathsf{E}/2 \end{pmatrix}, \tag{B6}$$

$$\mathsf{Q}_k = \begin{pmatrix} \mathsf{A} - 16\pi^2 D_x k^2 \mathsf{B} + 4F\pi k\mathrm{i}\mathsf{E} & 2\pi k\mathrm{i}\mathsf{E} \\ \pi(2k+1)\mathrm{i}\mathsf{E} & \mathsf{A} - 4\pi^2 D_x (2k+1)^2 \mathsf{B} + 2F\pi(2k+1)\mathrm{i}\mathsf{E} \end{pmatrix}, \tag{B7}$$

$$\mathsf{Q}_k^+ = \begin{pmatrix} \pi k\mathrm{i}\mathsf{E} & \mathsf{0} \\ \pi(2k+1)\mathrm{i}\mathsf{E} & \pi(2k+1)\mathrm{i}\mathsf{E}/2 \end{pmatrix}. \tag{B8}$$

We solve the recurrence relation for Equation B5 by introducing S_k and R_k that satisfy $\tilde{c}_{k+1} = \mathsf{S}_k \tilde{c}_k$ $(k \geq 0)$ and $\tilde{c}_{k-1} = \mathsf{R}_{k-1}\tilde{c}_k$ $(k \leq 0)$. With S_k and R_k, Equation B5 is calculated into

$$\mathsf{S}_{k-1} = -\left(\mathsf{Q}_k + \mathsf{Q}_k^+ \mathsf{S}_k\right)^{-1} \mathsf{Q}_k^- \quad (k \geq 1), \tag{B9}$$

$$\mathsf{R}_k = -\left(\mathsf{Q}_k^- \mathsf{R}_{k-1} + \mathsf{Q}_k\right)^{-1} \mathsf{Q}_k^+ \quad (k \leq -1), \tag{B10}$$

where S_k and R_k can be obtained by truncating at large k, namely at $k = -\tilde{M}_k, \tilde{M}_k (\approx M_k/2)$. For $k = 0$, we have

$$0 = \left[\mathsf{Q}_0^- \mathsf{R}_{-1} + \mathsf{Q}_0 + \mathsf{Q}_0^+ \mathsf{S}_0\right] \tilde{c}_0, \tag{B11}$$

where the first row of the left part of matrix in Equation B11 vanishes due to Equations B6–B8. Therefore, $\tilde{c}_0$ has a nontrivial solution and $\tilde{c}_k$ can be calculated by recursively applying S_k and R_k to $\tilde{c}_0$.

---

[1] R. Benzi, A. Sutera, and A. Vulpiani. The mechanism of stochastic resonance. *J. Phys. A*, 14:L453, 1981.

[2] B. McNamara and K. Wiesenfeld. Theory of stochastic resonance. *Phys. Rev. A*, 39:4854–4869, 1989.

[3] P. Jung and P. Hänggi. Amplification of small signals via stochastic resonance. *Phys. Rev. A*, 44:8032–8042, 1991.

[4] L. Gammaitoni, P. Hänggi, P. Jung, and F. Marchesoni. Stochastic resonance. *Rev. Mod. Phys.*, 70:223–287, 1998.

[5] M. D. McDonnell, N. G. Stocks, C. E. M. Pearce, and D. Abbott. *Stochastic resonance.* Cambridge University Press, 2008.

[6] M. D. McDonnell and D. Abbott. What is stochastic resonance? definitions, misconceptions, debates, and its relevance to biology. *PLoS Comput. Biol.*, 5:e1000348, 2009.

[7] F. Marchesoni, L. Gammaitoni, and A. R. Bulsara. Spatiotemporal stochastic resonance in a ϕ^4 model of kink-antikink nucleation. *Phys. Rev. Lett.*, 76:2609–2612, 1996.

[8] J. Teramae and D. Tanaka. Robustness of the noise-induced phase synchronization in a general class of limit cycle oscillators. *Phys. Rev. Lett.*, 93:204103, 2004.

[9] J. A. Acebrón, L. L. Bonilla, C. J. Pérez Vicente, F. Ritort, and R. Spigler. The Kuramoto model: A simple paradigm for synchronization phenomena. *Rev. Mod. Phys.*, 77:137–185, Apr 2005.

[10] H. Nakao, K. Arai, and Y. Kawamura. Noise-induced synchronization and clustering in ensembles of uncoupled limit-cycle oscillators. *Phys. Rev. Lett.*, 98:184101, 2007.

[11] M. Kœrn, T. C. Elston, W. J. Blake, and J. J. Collins. Stochasticity in gene expression: from theories to phenotypes. *Nat. Rev.*, 6:451–464, 2005.

[12] P. R. Patnaik. External, extrinsic and intrinsic noise in cellular systems: analogies and implications for protein synthesis. *Biotechnol. Mol. Biol. Rev.*, 1:121–127, 2006.

[13] N. Maheshri and E. K. O'Shea. Living with noisy genes: How cells function reliably with inherent variability in gene expression. *Annu. Rev. Biophys. Biomol. Struct.*, 36:413–434, 2007.

[14] J. Rausenberger, C. Fleck, J. Timmer, and M. Kollmann. Signatures of gene expression noise in cellular systems. *Prog. Biophys. Mol. Biol.*, 100:57–66, 2009.

[15] Y. Taniguchi, P. J. Choi, G.-W. Li, H. Chen, M. Babu, J. Hearn, A. Emili, and X. S. Xie. Quantifying *E. coli* proteome and transcriptome with single-molecule sensitivity in single cells. *Science*, 329:533, 2010.

[16] J. R. Chabot, J. M. Pedraza, P. Luitel, and A. van Oudenaarden. Stochastic gene expression out-of-steady-state in the cyanobacterial circadian clock. *Nature*, 450:1249–1252, 2007.

[17] D. Nozaki, D. J. Mar, P. Grigg, and J. J. Collins. Effects of colored noise on stochastic resonance in sensory neurons. *Phys. Rev. Lett.*, 82:2402–2405, Mar 1999.

[18] M. A. Fuentes, R. Toral, and H. S. Wio. Enhancement of stochastic resonance: the role of non Gaussian noises. *Physica A*, 295:114–122, 2001.

[19] M. O. Magnasco. Forced thermal ratchets. *Phys. Rev. Lett.*, 71:1477–1481, Sep 1993.

[20] P. Hänggi and F. Marchesoni. Artificial Brownian motors: Controlling transport on the

nanoscale. *Rev. Mod. Phys.*, 81:387–442, 2009.

[21] R. D. Astumian and M. Bier. Fluctuation driven ratchets: molecular motors. *Phys. Rev. Lett.*, 72:1766–1769, 1994.

[22] R. D. Astumian. Thermodynamics and kinetics of a Brownian motor. *Science*, 276:917–922, 1997.

[23] R. D. Astumian and I. Derényi. Fluctuation driven transport and models of molecular motors and pumps. *Eur. Biophys. J*, 27:474–489, 1998.

[24] T. Y. Tsong. Na, K-ATPase as a Brownian motor: Electirc field-induced conformational fluctuation leads to uphill pumping of cation in the absence of ATP. *J. Biol. Phys.*, 28:309–325, 2002.

[25] F. Marchesoni. Conceptual design of a molecular shuttle. *Phys. Lett. A*, 237:126–130, 1998.

[26] H. Linke, T. E. Humphrey, P. E. Lindelof, A. Lofgren, R. Newbury, P. Omling, A. O. Sushkov, R. P. Taylor, and H. Xu. Quantum ratchets and quantum heat pumps. *Appl. Phys. A*, 75:237–246, 2002.

[27] E. Lundh and M. Wallin. Ratchet effect for cold atoms in an optical lattice. *Phys. Rev. Lett.*, 94:110603, 2005.

[28] J. L. Mateos. A random walker on a ratchet. *Physica A*, 351:79–87, 2005.

[29] S. Bouzat and H. S. Wio. Current and efficiency enhancement in Brownian motors driven by non Gaussian noises. *Eur. Phys. J. B*, 41:97–105, 2004.

[30] S. E. Mangioni and H. S. Wio. A random walker on a ratchet potential: effect of a non Gaussian noise. *Eur. Phys. J. B*, 61:67–73, 2008.

[31] E. Frey and K. Kroy. Brownian motion: a paradigm of soft matter and biological physics. *Ann. Phys.*, 14:20–50, 2005.

[32] G. Wilk and Z. Włodarczyk. Interpretation of the nonextensivity parameter q in some applications of Tsallis statistics and Lévy distributions. *Phys. Rev. Lett.*, 84:2770–2773, Mar 2000.

[33] C. Beck. Dynamical foundations of nonextensive statistical mechanics. *Phys. Rev. Lett.*, 87:180601, Oct 2001.

[34] C. Beck and E. G. D. Cohen. Superstatistics. *Physica A*, 322:267–275, 2003.

[35] C. Beck. Generalized statistical mechanics for superstatistical systems. *Phil. Trans. R. Soc. A*, 369:453–465, 2011.

[36] C. Tsallis. Possible generalization of Boltzmann–Gibbs statistics. *J. Stat. Phys.*, 52:479–487, 1988.

[37] C. Tsallis. *Introduction to Nonextensive Statistical Mechanics: Approaching a Complex World*. Springer, 2009.

[38] S. M. D. Queirós and C. Tsallis. On the connection between financial processes with stochastic volatility and nonextensive statistical mechanics. *Eur. Phys. J. B*, 48:139–148, 2005.

[39] C. Beck. Superstatistical Brownian motion. *Prog. Theor. Phys. Suppl.*, 162:29–36, 2006.

[40] R. F. Rodríguez and I. Santamaría-Holek. Superstatistics of Brownian motion: A comparative study. *Physica A*, 385:456–464, 2007.

[41] P. Jizba and H. Kleinert. Superpositions of probability distributions. *Phys. Rev. E*, 78:031122, 2008.

[42] Y. Hasegawa and M. Arita. Bistable stochastic processes in the q-exponential family. *Physica A*, 389:4450–4461, 2010.

[43] G. C. Yalcin and C. Beck. Currents in complex polymers: An example of superstatistics for short time series. *Phys. Lett. A*, 376:2344–2347, 2012.

[44] Y. Hasegawa and M. Arita. Noise-intensity fluctuation in Langevin model and its higher-order Fokker–Planck equation. *Physica A*, 390:1051–1063, 2011.

[45] Y. Hasegawa and M. Arita. Escape process and stochastic resonance under noise-intensity fluctuation. *Phys. Lett. A*, 375:3450–3458, 2011.

[46] P. Reimann, R. Bartussek, R. Häußler, and P. Hänggi. Brownian motors driven by temperature oscillations. *Phys. Lett. A*, 215:26–31, 1996.

[47] Y.-X. Li. Transport generated by fluctuating temperature. *Physica A*, 238:245–251, 1997.

[48] Y. Zhang and J. Chen. Investigation on a temporal asymmetric oscillating temperature ratchet. *Physica A*, 387:3443–3448, 2008.

[49] M. Borromeo, S. Giusepponi, and F. Marchesoni. Recycled noise rectification: An automated Maxwell's deamon. *Phys. Rev. E*, 74:031121, 2006.

[50] W. A. M. Morgado, S. M. D. Queirós, and D. O. Soares-Pinto. On exact time averages of a massive Poisson particle. *J. Stat. Mech.*, page P06010, 2011.

[51] C. R. Doering and J. C. Gadoua. Resonant activation over a fluctuating barrier. *Phys. Rev. Lett.*, 69:2318–2321, Oct 1992.

[52] R. N. Mantegna and B. Spagnolo. Noise enhanced stability in an unstable system. *Phys. Rev.*

Lett., 76:563–566, Jan 1996.

[53] B. Spagnolo, N. V. Agudov, and A. A. Dubkov. Noise enhanced stability. *Acta Phys. Pol. B*, 35:1419–1436, 2004.

[54] N. Rosenfeld, J. W. Young, U. Alon, P. S. Swain, and M. B. Elowitz. Gene regulation at the single-cell level. *Science*, 307:1962–1965, 2005.

[55] M. J. Dunlop, R. S. C. III, J. H. Levine, R. M. Murray, and M. B. Elowitz. Regulatory activity revealed by dynamic correlations in gene expression noise. *Nature Genetics*, 40:14393–1498, December 2008.

[56] R. Bartussek, P. Reimann, and P. Hänggi. Precise numerics versus theory for correlation ratchets. *Phys. Rev. Lett.*, 76:1166–1169, 1996.

[57] B. Lindner, L. Schimansky-Geier, P. Reimann, P. Hänggi, and M. Nagaoka. Inertia ratchets: A numerical study versus theory. *Phys. Rev. E*, 59:1417–1424, 1999.

[58] H. Risken. *The Fokker–Planck Equation: Methods of Solution and Applications*. Springer, 2nd edition, 1989.

[59] M. Scott, B. Ingalls, and M. Kærn. Estimations of intrinsic and extrinsic noise in models of nonlinear genetic networks. *Chaos*, 16:026107, 2006.

[60] V. Shahrezaei, J. F. Ollivier, and P. S. Swain. Colored extrinsic fluctuations and stochastic gene expression. *Mol. Syst. Biol.*, 4:196, 2008.

[61] V. Kampen. *Stochastic Process Theory in Physics and Chemistry*. North-Holland, 1992.